OPEN

Novel hetero-layered materials with tunable direct band gaps by sandwiching different metal disulfides and diselenides

Humberto Terrones[1], Florentino López-Urías[1]* & Mauricio Terrones[1,2]

[1]Department of Physics & Center for 2-Dimensional and Layered Materials, The Pennsylvania State University, University Park, PA 16802, USA, [2]Department of Materials Science and Engineering and Materials Research Institute, The Pennsylvania State University, University Park, PA 16802, USA.

Although bulk hexagonal phases of layered semiconducting transition metal dichalcogenides (STMD) such as MoS_2, WS_2, WSe_2 and $MoSe_2$ exhibit indirect band gaps, a mono-layer of STMD possesses a direct band gap which could be used in the construction of novel optoelectronic devices, catalysts, sensors and valleytronic components. Unfortunately, the direct band gap only occurs for mono-layered STMD. We have found, using first principles calculations, that by alternating individual layers of different STMD (MoS_2, WS_2, WSe_2 and $MoSe_2$) with particular stackings, it is possible to generate direct band gap bi-layers ranging from 0.79 eV to 1.157 eV. Interestingly, in this direct band gap, electrons and holes are physically separated and localized in different layers. We foresee that the alternation of different STMD would result in the fabrication of materials with unprecedented optical and physico-chemical properties that would need further experimental and theoretical investigations.

T ransition metal dichalcogenides (TMD) form bulk layered materials in which the layers interact via van der Waals forces, similar to graphene and hexagonal boron nitride (h-BN). This is why TMD are good solid lubricants, including inorganic Fullerenes and nanotubes of MoS_2 and WS_2[1–3]. Recently, the electronic properties of few-layered MoS_2, WS_2 and WSe_2 have been measured[4–7]. It is important to note that monolayers of TMD are not single-atom thick, as in graphene or h-BN, but instead they are formed by layers in which the transition metal atom (W or Mo) is sandwiched between sulfur or selenium atoms (see figure 1). The TMD phases possess two types of atomic arrangements: the trigonal prismatic and the octahedral[8], and they could either exhibit semiconducting (e.g. MoS_2, WS_2, WSe_2 and $MoSe_2$) or metallic-superconducting behavior (e.g. NbS_2 and $NbSe_2$)[9–13]. Normally, the bulk hexagonal phases (trigonal prismatic) of semiconducting TMD (STMD) reveal an indirect band gap from the Γ point to an intermediate point in the Brillouin zone (Γ-I) (see figure 2a); the result has been also confirmed by first principles calculations[14–18]. Heinz and co-workers have found that mono-layers of MoS_2 strongly emit light due to a 1.8 eV direct band gap at the K point in the Brillouin zone[19]. This direct gap has also been confirmed experimentally by other groups through photoluminescence in exfoliated MoS_2[20–22] and chemical vapor deposition islands of monolayer WS_2; for this case the direct band gap is around 1.9 eV[23] (see figure 2b). Besides the transformation to a direct band gap for a monolayer of STMD, a break of inversion symmetry also occurs[24], which has been confirmed experimentally by circularly polarized light experiments that lead to valley polarization effects[25,26]. To date, various groups have performed first principles calculations using Local density approximation (LDA), Generalized gradient approximation-Perdew-Burke-Ernzerhof (GGA-PBE), Hybrid-DFT Heyd-Scuseria-Ernzerhof (HSE), many body perturbation theory under the GW approximation (including excitonic and spin orbit coupling effects), in order to obtain the band structure with more precision and explain the experimental reported observations[15–17,27–32]. Although there are differences in the band gaps due to the particular theoretical approach used, all these calculations agree in the main features of the band structure and in the existence of direct band gaps for monolayers of STMD and indirect gaps in bilayers and multilayer systems.

When a second layer of the same dichalcogenide is added to the monolayer, the indirect band gap from the Γ point to an intermediate state (Γ-I) becomes significant[17], and the system loses the direct band gap character.
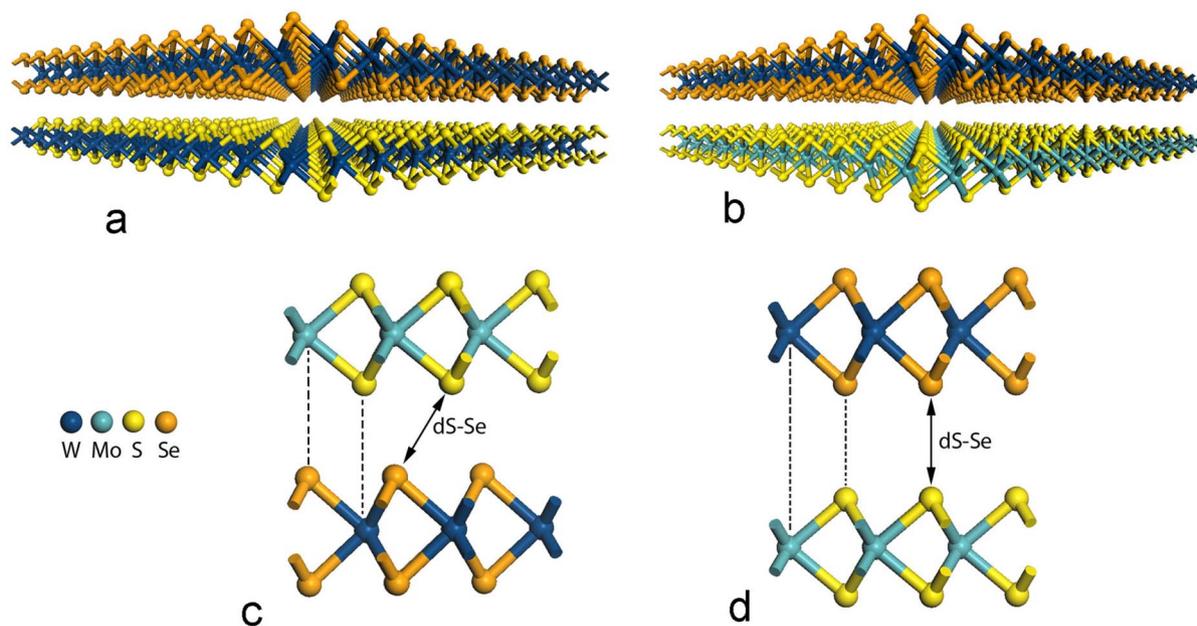
Figure 1 | **Atomic models representing the bilayer heterostructures of semiconducting transition metal dichalcogenides (STMD).** (a) Bilayers formed by overlapping WSe_2 on WS_2 with stacking type B (bulk) denoted as Bilayer (WS_2, WSe_2, B); (b) Bilayer formed by placing WSe_2 on MoS_2 with stacking type A denoted as Bilayer (MoS_2, WSe_2, A); (c) Staking type B in which the transition metal atoms are on top of the chalcogen atoms. This is the stacking found in bulk STMD, and (d) Stacking type A in which the chalcogen atoms are on top of each other. The dotted lines indicate the alignment of atoms between layers, and the arrows correspond to the distance dS-Se between chalcogen atoms of different layers (see supplementary information table 2S).

Therefore, the direct band gap at the K point is restricted to monolayers of STMD. In order to understand further this issue, we have also performed first principles calculations on different stackings and rotations of one layer with respect to another in the bilayer systems of the same dichalcogenide, and found the absence of a direct band gap even for twisted bilayers. However, and to our surprise, when considering the stacking of different bilayers of STMD (e.g. WS_2-MoS_2, WSe_2-MoS_2 $MoSe_2$-MoS_2, WSe_2-$MoSe_2$, etc.), the direct band gap at the K point becomes dominant, similar to monolayers. Moreover, in some of these geometries we found that the alternated layers can result in an infinite hybrid crystal with a direct band gap. In our study, and according to the band structure analysis, we described the main features such as the presence of a direct band gap at the K point, as well as the presence of particular indirect gaps. In this context, we have identified four families of hybrid STMD: WS_2-MoS_2 as type 1, WSe_2-WS_2 and WSe_2-MoS_2 as type 2, $MoSe_2$-WS_2 and $MoSe_2$-MoS_2 as type 3 and WSe_2-$MoSe_2$ as type 4 (see figure 1).

Results

Family of Hybrids WS_2-MoS_2 (type 1). For all the performed first principles calculations, we selected two types of stackings to overlap the monolayers of STMD: First, we considered the crystal stacking found in the bulk phases; the letter B (bulk) is used to indicate this type of stacking. In particular, for stacking type B, the S (Se) atoms of one layer sit on top of the metal atoms of the other layer (see figures 1a and 1c). The second stacking contemplated in our study, consists of S (Se) atoms arranged on top of the S (Se) atoms of the adjacent layer (see figures 1b and 1d); we refer to this case as A stacking.

For the hybrid layers of MoS_2 and WS_2 arranged in a bilayer with a stacking type B, we introduced the notation: bilayer (MoS_2, WS_2, B); in which the first two symbols within the brackets refer to the STMD considered and the next symbol indicates the stacking type (A or B). We have also considered infinite crystal cases (infinite number of layers) with stackings type A and B as crystal (MoS_2, WS_2, A) and crystal (MoS_2, WS_2, B), respectively. We find for all the cases of this

family (hybrids MoS_2-WS_2), the absence of a dominant direct band gap. It is worth mentioning that the gap difference between the direct gap at K and indirect gap Γ-I for the A stackings is reduced when compared to the corresponding difference in stackings of type B (see table 1 and figure 2c). This gap reduction is due to an increase in the indirect gap at Γ-I for the stacking A cases. The direct gap at the K point changes very little in these systems, from 1.664 eV for crystal (MoS_2, WS_2, B) to 1.708 eV for bilayer (MoS_2, WS_2, B), whereas the indirect gap Γ-I changes more dramatically from 0.764 eV in the crystal (MoS_2, WS_2, B) to 1.586 eV for the bilayer (MoS_2, WS_2, A). Regarding stability, the total energy/cell (one cell contains one unit of WS_2 and one unit of MoS_2) always favors the stackings type B with a difference of 0.1138 eV/cell for the crystals and 0.0744 eV/cell for the bilayers (see table 1S in supplementary information). The lattice parameters "a" for this family varies very little from 3.155 Å for the bilayer (MoS_2, WS_2, A) to 3.158Å for the crystal (MoS_2, WS_2, B), thus lying between the lattice constants of WS_2 and MoS_2 crystals[33] (see table 2S in supplementary information). The bond lengths (Mo-S and W-S) are basically the same as in the corresponding monolayer (see table 3S in supplementary information).

Family of Hybrids WS_2-WSe_2 and MoS_2-WSe_2 (type 2). Interestingly, when mixing layers of WS_2 and WSe_2 a direct gap behavior at K is obtained for bilayer stackings A and B (see table 1, figure 2d, figure 2f and figure 1S in supplementary information). Therefore, the direct gap is smaller than their corresponding indirect gaps at Γ-I. Although the direct gaps at K for this family are around 1 eV, the indirect gaps within Γ-I change from 0.883 eV for the crystal (WS_2, WSe_2, B) to 1.725 eV for the bilayer (WS_2, WSe_2, A) (see table 1). Surprisingly, the crystal formed by an infinite number of stacked layers in the A fashion, crystal (WS_2, WSe_2, A), exhibits a direct band gap at K, being this the first case of a multilayer STMD system with a direct band gap behavior (see figure 2f). Note that the direct band gaps for this family, around 1.0 eV (1239.84 nm), are reduced with respect to the direct band gaps for monolayers of WS_2 (1.94 eV or 639.09 nm), and WSe_2 (1.67 eV or 742.42 nm)
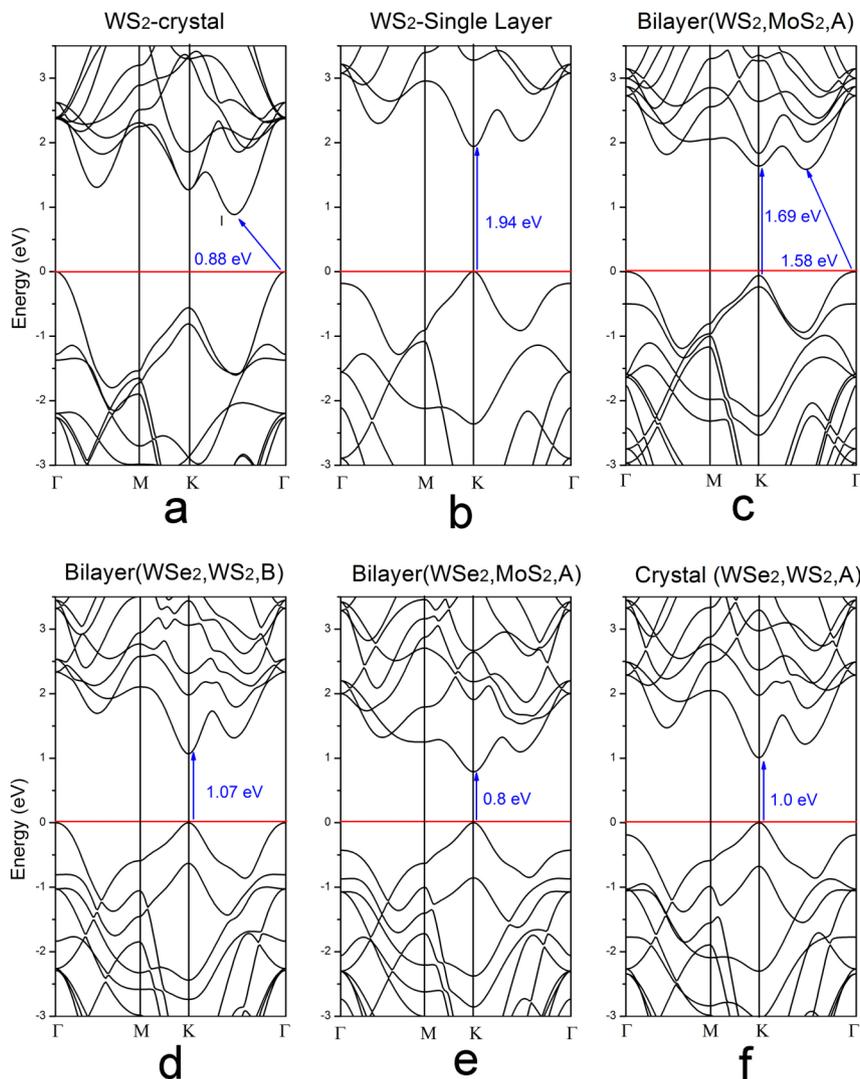
Figure 2 | (a) Band structure of bulk hexagonal WS_2 (The blue arrow shows the indirect gap Γ-I); (b) Band structure of a monolayer of WS_2 (note the blue arrow revealing the direct band gap location); (c) Type 1 family of WS_2-MoS_2 showing the band structure of the bilayer with an A stacking; (d) Type 2 family band structure showing the direct band gap of bilayer (WS_2, WSe_2, B); (e) Type 2 family band structure of the direct band gap corresponding to the bilayer (WSe_2, MoS_2, A), and (f) the Type 2 family, band structure of the infinite number of layers case: Crystal (WS_2, WSe_2, A). The red line indicates the top of the valence band.

(see table 4S in supplementary information), thus widening the possibilities of applications for STMD in the infrared range.

In order to analyze deeply the nature of the direct band gap, the partial density of states (PDOS) considering the d-electrons of the transition metal and the p-electrons of the chalcogen atoms were calculated (see figures 3a, b, c and 1S in supplementary information). The results indicate that the states at the top of the valence band, for the bilayer case (WS_2-WSe_2, A), are due to the W and Se of the WSe_2 layer, and those at bottom of the conduction band are owed to the W

and S of the WS_2 layer. Therefore, electrons and holes are physically separated by the two different layers which constitute the TMD bilayer. A similar behavior has been found theoretically in h-BN nanotubes and homogeneous layered TMD when applying an external electric field; the so called Giant Stark Effect (GSE)[31,34]. In GSE the electric field separates physically electrons and holes and also helps the reduction of the band gap. However, in our hetero-geneous TMD bilayers there is no external electric field applied, but it has been found, for the direct band gap bilayers, that although there is

Table 1 | Direct and indirect (in parenthesis) band gaps in eV of hybrids of semiconducting transition metal dichalcogenides (STMD). Systems with a dominant direct band gap at the K point in the Brillouin zone have an asterisk. Cases with "+" show an indirect fundamental band gap Γ-K, and "&" corresponds to a dominant indirect gap K-I

Hybrid-Structure	Bilayer-Stacking A	Bilayer-Stacking B	Crystal- stacking A	Crystal- stacking B
WS_2-MoS_2 Type 1	1.695(1.586 Γ-I)	1.708(1.190 Γ-I)	1.669(1.284 Γ-I)	1.664 (0.764 Γ-I)
WS_2-WSe_2 Type 2	1.007(1.725 Γ-I)*	1.068(1.314 Γ-I)*	1.007(1.406 Γ-I)*	1.037 (0.883 Γ-I)
MoS_2-WSe_2 Type 2	0.790(1.525 Γ-I)*	0.891(1.147 Γ-I)*	0.802(1.245 Γ-I)*	0.883 (0.736 Γ-I)
WS_2-$MoSe_2$ Type 3	1.154(1.594 Γ-I)*	1.180(1.052 Γ-K)+	1.157(1.316 Γ-I)*	1.155 (0.790 Γ-I)
MoS_2-$MoSe_2$ Type 3	0.945(1.560 Γ-I)*	1.013(0.899 Γ-K)+	0.949(1.260 Γ-I)*	0.998 (0.699 Γ-I)
WSe_2-$MoSe_2$ Type 4	1.443(1.330 K-I)&	1.471(1.116 Γ-I)	1.444(1.215 K-I)&	1.418 (0.761 Γ-I)
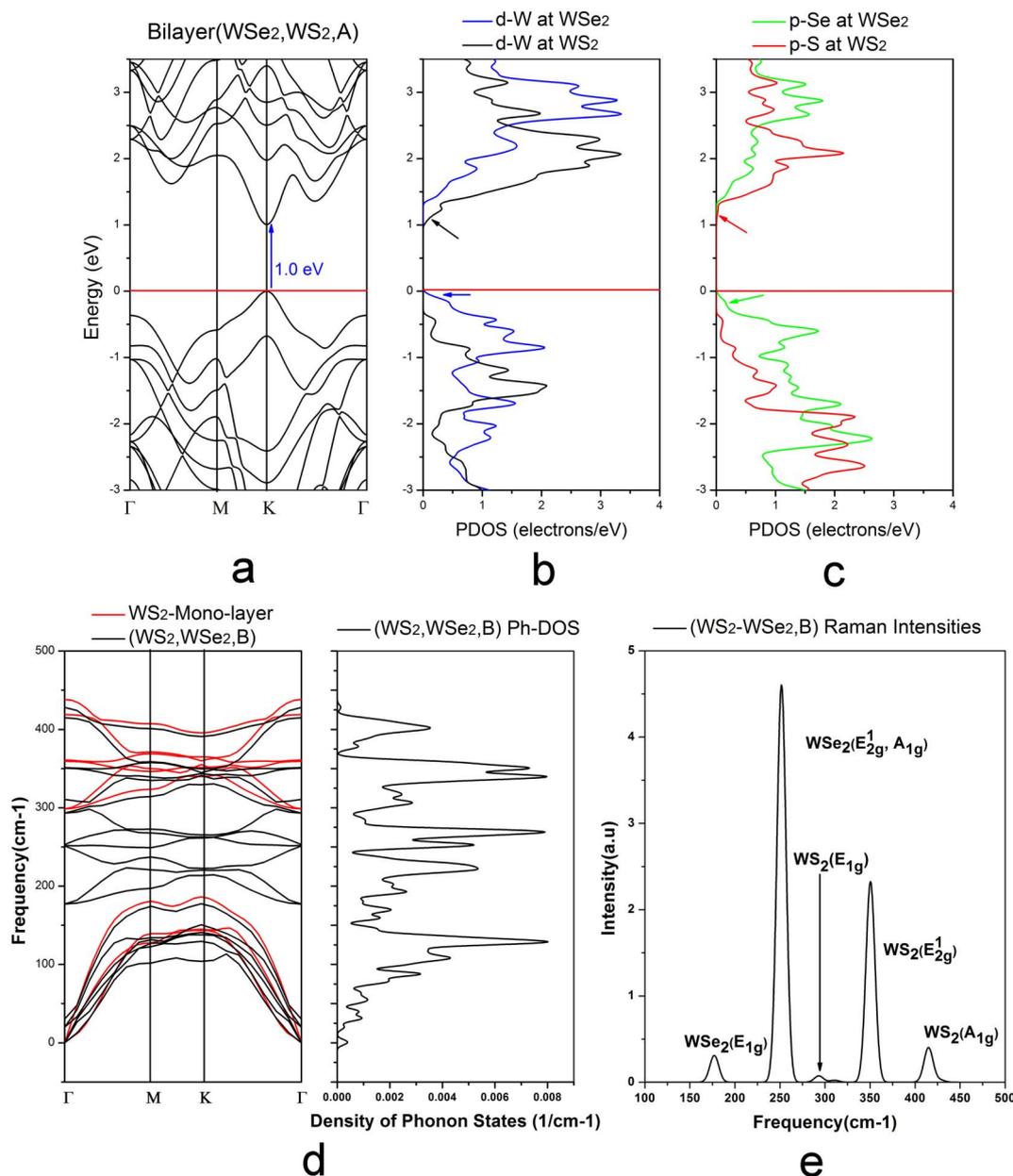
Figure 3 | Type 2 Bilayer (WSe$_2$, WS$_2$, A): (a) Band structure showing the direct band gap; (b) PDOS showing the d-electrons of W at each of the layers. The blue arrow indicates the states at the top of the valence band caused by W in the WSe$_2$ layer, and the black arrow shows the states at bottom of the conduction band due to W in the WS$_2$ layer; (c) PDOS showing the p-electrons of the chalcogen atoms. The green arrow exhibits the states at the top of the valence band of Se in the WSe$_2$ layer, and the red arrow reveals the states at the bottom of the conduction band of the S atoms in the WS$_2$ layer; (d) DFT-LDA calculated phonon dispersion for the WS$_2$ monolayer in red, and the bilayer (WS$_2$, WSe$_2$, B) in black. The phonon density of states is shown (right hand side), and (e) DFT-LDA Raman intensities due to the different phonon modes in the bilayer (WS$_2$-WSe$_2$, B) using a laser wave length of 514.5 cm^{-1} at 300 K.

charge neutrality in the whole system, the local Mulliken charges for the transition metal atoms, as well as for the chalcogen atoms, possess different sign in different layers. For example, for the bilayer (WS$_2$-WSe$_2$, A), the W of the WS$_2$ layer exhibits a positive net charge ($+0.16$ e), whereas the W of the WSe$_2$ layer reveals a negative net charge (-0.09 e). Similarly, the S atoms of the WS$_2$ layer exhibit a negative net charge, and the Se show a positive net charge. This is not the case, for indirect band gap bilayers sharing the same chalcogen atom, as found in bilayer (WS$_2$, MoS$_2$, B) systems, in which both Mo and W atoms display the same charge sign as well as the S and Se atoms. Therefore, an intrinsic electric field might be the cause of the electron-hole separation and the presence of the direct band gap.

Since one of the most important experimental tools for characterizing few layer TMD systems is Raman spectroscopy[4,5,20,22,23,35], the phonon dispersion, the phonon density of states and the Raman intensities have been calculated using density functional perturbation theory for the bilayer (WS$_2$-WSe$_2$, B) (see figure 3d and e). When compared to the WS$_2$ monolayer, the phonon dispersion of the bilayer exhibits a shift which might be caused by the expansion of the WS$_2$ lattice when interacting with the WSe$_2$ layer. From the phonon dispersion and the Raman intensities, it is possible to identify the main phonon modes and their positions: E$_{1g}$ (176.99 cm^{-1} for WSe$_2$ and 293.23 for WS$_2$), E$_{2g}^1$ (251.33 cm^{-1} for WSe$_2$ and 350.50 cm^{-1} for WS$_2$) and A$_{1g}$ (251.80 cm^{-1} for WSe$_2$ and

414.93 for WS$_2$. See figure 3e). Note that the E$_{2g}^1$ and the A$_{1g}$ for the WSe$_2$ are almost degenerate as has been found experimentally in bulk WSe$_2$ (250 cm^{-1} for E$_{2g}^1$ and 253 cm^{-1} for A$_{1g}$)[36].

The crystal formed by alternating layers with the stacking type B, crystal (WS$_2$, WSe$_2$, B), always exhibits an indirect gap at Γ-I (see table 1). The bilayer (WS$_2$, WSe$_2$, B) is more stable by 0.0758 eV/Cell when compared to the bilayer (WS$_2$, WSe$_2$, A). For the infinite crystal cases, crystal (WS$_2$, WSe$_2$, B) is more stable by 0.1494 eV/cell than crystal (WS$_2$, WSe$_2$, A) (see table 1S supplementary information), and the lattice parameter of this family is *ca.* 3.20Å (see table 2S supplementary information). The bond lengths W-S are around 2.413 Å, slightly larger than for the WS$_2$ monolayer. At the same time, a slight reduction in the W-Se distances is observed when compared to the monolayer from 2.519 Å to 2.510 Å (see table 3S in supplementary information).

Bilayer systems of MoS$_2$-WSe$_2$, exhibit a direct gap with A and B stackings, as well as the infinite crystal with the A stacking (see figure 2e). However, the direct gap values for these cases are *ca.* 0.8 eV (1549.8 nm) (see table 1). The indirect gap Γ-I varies from 0.736 eV for the crystal (MoS$_2$, WSe$_2$, B) to 1.525 eV for bilayer (MoS$_2$, WSe$_2$, A). With regard to the energetics, the crystal (MoS$_2$, WSe$_2$, B) is more stable than the crystal (MoS$_2$, WSe$_2$, A) by 0.1613 eV/Cell, and for the bilayer cases, the crystal stacking B is more stable than the A stacking by 0.0816 eV/cell (see table 1S supplementary information). The lattice parameter "a" of this family ranges between 3.218Å and 3.22Å (see table 2S supplementary information). Here, the Mo-S distance increases to 2.430 Å compared to the MoS$_2$ monolayer (2.417 Å), and the W-Se decreases slightly around 0.008 Å (see table 3S in supplementary information).

Family of Hybrids WS$_2$-MoSe$_2$ and MoS$_2$-MoSe$_2$ (Type 3). The hybrid cases consisting of WS$_2$ -MoSe$_2$ layers and MoS$_2$-MoSe$_2$ layers share similarities. First, both of them exhibit dominant direct band gaps when stacked in the A fashion (Bilayer and infinite layers. See table 1). Both bilayer cases are indirect gap Γ-K materials when exhibiting staking type B (see figures 4a and 4b). Note that for the previous cases, the indirect gap occurred at Γ-I (see table 1). This hybrid system (type 3) could exhibit three electronic
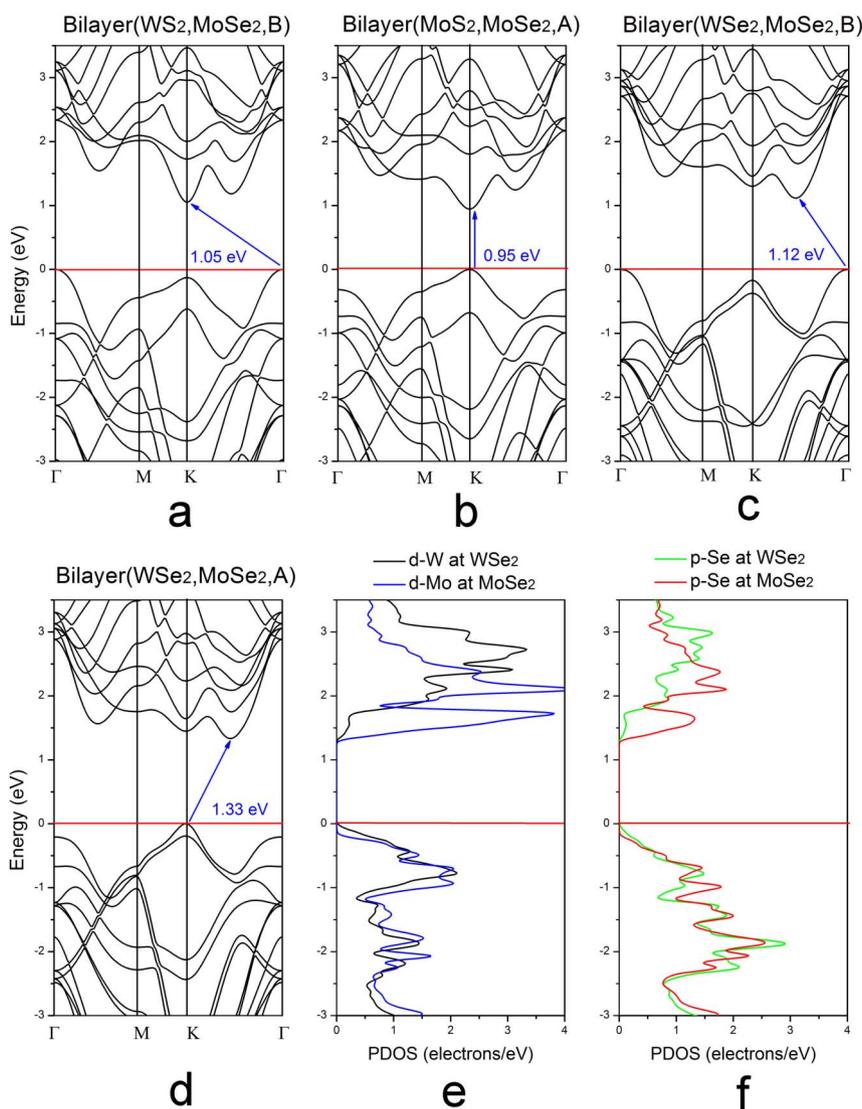
Figure 4 | (a) Type 3 family band structure of the bilayer (WS$_2$, MoSe$_2$, B) showing the Γ-K band gap; (b) Type 3 band structure showing the direct band gap for the bilayer (MoS$_2$, MoSe$_2$, A); (c) Type 4 family band structure of the bilayer (WSe$_2$, MoSe$_2$, B) exhibiting an indirect band gap Γ-I; (d) Type 4 family Bilayer (WSe$_2$, MoSe$_2$, A) band structure showing the indirect band gap K-I, and (e) PDOS of Bilayer (WSe$_2$, MoSe$_2$, A) showing the d-electrons of W and Mo at each of the layers. Note that the states at the top of the valence band are mainly due to W in the WSe$_2$ layer, and the Mo in the MoSe$_2$ layer provides more states than W; (c) PDOS of Bilayer (WSe$_2$, MoSe$_2$, A) showing the states due to the p-electrons of the chalcogen atoms.

behaviors: Direct gap at K, indirect gap Γ-I and indirect gap Γ-K. This result enriches the possibilities of creating novel hetero-layered nanostructures exhibiting unprecedented physico-chemical properties.

In addition, the direct band gap for the WS_2-$MoSe_2$ cases varies from 1.154eV (1074.38nm) for the bilayer (WS_2, $MoSe_2$, A) case to 1.180 eV (1050.71 nm) for the bilayer (WS_2, $MoSe_2$, B) which does not have a fundamental direct gap, but an indirect gap Γ-K (see table 1). The indirect gap at Γ-K is 1.052 eV for the bilayer (WS_2, $MoSe_2$, B), and the indirect gap at Γ-I changes from 0.790 eV for the crystal (WS_2, $MoSe_2$, B) to 1.594 eV for the bilayer (WS_2, $MoSe_2$, A). The most stable cases correspond to the stacking type B, being more favorable by 0.1517 eV/cell the crystal (WS_2, $MoSe_2$, B) than the crystal (WS_2, $MoSe_2$, A). The bilayer (WS_2, $MoSe_2$, B) is more stable by 0.0768 eV/cell when compared to the bilayer (WS_2, $MoSe_2$, A) (see table 1S supplementary information). The lattice parameter "a" for this family is around 3.21Å (see table 2S supplementary information).

The situation for the MoS_2-$MoSe_2$ family is similar to the previous system described, but exhibiting a direct gap at *ca.* 0.945 eV (1312.00 nm) (see figure 4b). The indirect gap Γ-I changes from 0.699 eV for crystal (MoS_2, $MoSe_2$, B) to 1.560 eV for bilayer (MoS_2, $MoSe_2$, A) (See table 1). The crystal (MoS_2, $MoSe_2$, B) is more stable by 0.1645 eV/cell than crystal (MoS_2, $MoSe_2$, A). The bilayer (MoS_2, $MoSe_2$, A) is less stable than bilayer (MoS_2, $MoSe_2$, B) by 0.0834 eV/cell (see table 1S supplementary information). The lattice parameter "a" is 3.225Å for the bilayer (MoS_2, $MoSe_2$, A), with little change for the crystal (MoS_2, $MoSe_2$, B), being 3.228Å (see table 2S supplementary information). For the type 3 family, the metal-sulfur distances increase and the metal-selenium distances decrease with respect to their corresponding monolayers (see table 3S in supplementary information).

Family of Hybrids WSe_2-$MoSe_2$ (Type 4). For the cases studied using overlapped layers of WSe_2 and $MoSe_2$, there is no direct band gap smaller than the indirect gaps at Γ-I and K-I, condition that needs to be satisfied in order to have a fundamental direct band gap material. For bilayer (WSe_2, $MoSe_2$, A), the direct gap at the K point is smaller (1.443 eV) than the indirect gap Γ-I (1.538 eV), but not smaller than the indirect gap at K-I (1.330 eV). Thus, the material possesses an indirect gap at K-I (see table 1 and figure 4d). The PDOS of bilayer (WSe_2, $MoSe_2$, A) shows that the states at the top of the valence band are slightly dominated by the WSe_2 layer (W d-electrons, and Se p-electrons); however, the bottom of the conduction band exhibits states from both layers, with more states arising from the $MoSe_2$ layer (see figure 4e and 4f).

The crystal (WSe_2, $MoSe_2$, A) also exhibits a K-I band gap of 1.215eV (see table 1). The other two cases: bilayer (WSe_2, $MoSe_2$, B) and crystal (WSe_2, $MoSe_2$, B), reveal indirect band gaps Γ-I (see figure 4e). The relative stability of the crystalline cases indicates that the crystal (WSe_2, $MoSe_2$, B) is more stable than crystal (WSe_2, $MoSe_2$, A) by 0.1632 eV/Cell. For bilayers, the bilayer (WSe_2, $MoSe_2$, B) is more stable by 0.0826 eV/cell than bilayer (WSe_2, $MoSe_2$, A) (see table 1S supplementary information). The lattice parameter "a" of this family is the largest of all studied STMD with 3.28Å for the crystal (WSe_2, $MoSe_2$, B). This cell parameter is very close to that reported experimentally for WSe_2 and $MoSe_2$ crystals[37,38] (see tables 2S and 4S supplementary information). The bond distance of W-Se exhibits a slight increase (2.521 Å) when compared to the corresponding distance of the monolayer (2.519 Å). The distance Mo-Se is basically preserved when compared to the monolayer (see table 3S in supplementary information).

Discussion

To the best of our knowledge, we have demonstrated for the first time, that it is indeed possible to obtain novel direct band gap bilayers of STMD if different monolayers are overlapped. Moreover, in some cases it is possible to even have direct band gap crystals with infinite number of layers if the stacking belongs to A type. It has been found that the direct band gap bilayers exhibit a physical separation of electron and holes probably due to a sort of local Giant Stark Effect caused by charge differences established between the hetero-geneous layers. In these systems, the top the valence band is dominated by the selenide layer and the bottom of the conduction band is controlled by the states of the sulfide layer. Homogeneous bilayers of TMD do not possess this net charge separation and hence do not exhibit direct band gaps. In addition, this is a different behavior from that found for monolayers of STMD, in which electrons and holes are restricted to interact within the layer.

In particular, the family of WS_2-WSe_2 and MoS_2-WSe_2 layers, is the most interesting since the bilayer behaves like a direct band gap material for the two stackings considered in this manuscript (A and B; being B the most stable). These 2D layered systems could be synthesized by sandwiching exfoliated monolayers or chemical vapor deposition layers, using a careful transfer of the monolayers. Moreover, this family could also produce a direct band gap crystal with A stacking. In addition, we have found that the family of hybrids WS_2-$MoSe_2$ and MoS_2-$MoSe_2$, besides having a direct band gap for A stackings, they exhibit an indirect gap at Γ-K for a bilayer with stacking type B; result which has not been reported hitherto for STMD. Another relevant feature is that the distance between layers increases for type A stackings, found to be the least favorable energetically speaking (see table 1S supplementary information). However, by twisting the layers or by changing the stacking, new cases with more favorable energetics could be found. It is important to mention that the direct band gaps of the hybrid systems studied in this account range from 0.79 eV (1569.42 nm) to 1.15 eV (1078.12 nm), which are much smaller than the direct band gaps, already found experimentally in monolayers of WS_2 (2.1 eV) and MoS_2 (1.8 eV)[9]. Certainly, there is more work to be carried out, not only experimentally, but theoretically by studying the spin-orbit coupling in bilayer TMDS, as well as carrying out GW calculations considering excitonic effects. Finally, the novel hybrid bilayer systems exhibit new optical properties useful for applications in the infrared range. With the hybrid layer technology at hand, it would be possible to experimentally produce bilayer hybrid systems with novel photoluminescence properties. Note that in these bilayer systems there is no inversion symmetry, so they might play an important role in valley polarization and valleytronics.

Methods

1. Fleischauer, P. D. Fundamental-Aspects of the Electronic-Structure, Materials Properties and Lubrication Performance of Sputtered MoS_2 Films. *Thin Solid Films* **154**, 309–322 (1987).
2. Martin, J. M., Donnet, C., Lemogne, T. & Epicier, T. Superlubricity of Molybdenum-Disulfide. *Phys. Rev. B* **48**, 10583–10586 (1993).
3. Rapoport, L., Fleischer, N. & Tenne, R. Applications of WS_2 (MoS_2) inorganic nanotubes and fullerene-like nanoparticles for solid lubrication and for structural nanocomposites. *J. Mater. Chem.* **15**, 1782–1788 (2005).
4. Hwang, W. S. et al. Transistors with chemically synthesized layered semiconductor WS_2 exhibiting 10^5 room temperature modulation and ambipolar behavior. *Applied Physics Letters* **101** (2012).
5. Wang, H. et al. Integrated Circuits Based on Bilayer MoS_2 Transistors. *Nano Letters* **12**, 4674–4680 (2012).
6. Zhang, Y. J., Ye, J. T., Matsuhashi, Y. & Iwasa, Y. Ambipolar MoS_2 Thin Flake Transistors. *Nano Letters* **12**, 1136–1140 (2012).
7. Fang, H. et al. High-Performance Single Layered WSe_2 p-FETs with Chemically Doped Contacts. *Nano Letters* **12**, 3788–3792 (2012).
8. Wieting, T. K., Schluter. in *Physics and Chemistry of Materials with Layered Structures* (ed E. Mooser) (D. Reidel, Boston, 1979).
9. Wang, Q. A., Kalantar-Zadeh, K., Kis, A., Coleman, J. N. & Strano, M. S. Electronics and optoelectronics of two-dimensional transition metal dichalcogenides. *Nature Nanotechnology* **7**, 699–712 (2012).
10. Kam, K. K. & Parkinson, B. A. Detailed Photocurrent Spectroscopy of The Semiconducting Group-VI Transition-Metal Dichalcogenides. *Journal of Physical Chemistry* **86**, 463–467 (1982).
11. Beal, A. R., Hughes, H. P. & Liang, W. Y. Reflectivity Spectra of Some VA Transition-Metal Dichalcogenides. *Journal of Physics C-Solid State Physics* **8**, 4236–4248 (1975).
12. Traving, M. et al. Electronic structure of WSe_2: A combined photoemission and inverse photoemission study. *Phys. Rev. B* **55**, 10392–10399 (1997).
13. Finteis, T. et al. Occupied and unoccupied electronic band structure of WSe_2. *Phys. Rev. B* **55**, 10400–10411 (1997).
14. Mattheis, L. F. Energy-Bands For 2H-$NbSe_2$ AND 2H-MoS_2. *Physical Review Letters* **30**, 784–787 (1973).
15. Boker, T. et al. Band structure of MoS_2, $MoSe_2$, and alpha-$MoTe_2$: Angle-resolved photoelectron spectroscopy and ab initio calculations. *Phys. Rev. B* **64** (2001).
16. Jiang, H. Electronic Band Structures of Molybdenum and Tungsten Dichalcogenides by the GW Approach. *Journal of Physical Chemistry C* **116**, 7664–7671 (2012).
17. Cheiwchanchamnangij, T. & Lambrecht, W. R. L. Quasiparticle band structure calculation of monolayer, bilayer, and bulk MoS_2. *Phys. Rev. B* **85** (2012).
18. Enyashin, A., Gemming, S. & Seifert, G. Nanosized allotropes of molybdenum disulfide. *European Physical Journal-Special Topics* **149**, 103–125 (2007).
19. Mak, K. F., Lee, C., Hone, J., Shan, J. & Heinz, T. F. Atomically Thin MoS_2: A New Direct-Gap Semiconductor. *Physical Review Letters* **105** (2010).
20. Splendiani, A. et al. Emerging Photoluminescence in Monolayer MoS_2. *Nano Letters* **10**, 1271–1275 (2010).
21. Korn, T., Heydrich, S., Hirmer, M., Schmutzler, J. & Schuller, C. Low-temperature photocarrier dynamics in monolayer MoS_2. *Applied Physics Letters* **99** (2011).
22. Eda, G. et al. Photoluminescence from Chemically Exfoliated MoS_2. *Nano Letters* **11**, 5111–5116 (2011).
23. Gutierrez, H. R., Perea-Lopez, N., Elias, A. L., Berkdemyr, A., Wang, B., LV, R., Lopez-Urias, F., Crespi, V. H., Terrones, H. & Terrones, M. Extraordinary Room-Temperature Photoluminescence in Triangular WS_2 Monolayers. *Nano Letters*. DOI 10.1021/nl3026357 (2012).
24. Xiao, D., Liu, G. B., Feng, W. X., Xu, X. D. & Yao, W. Coupled Spin and Valley Physics in Monolayers of MoS_2 and Other Group-VI Dichalcogenides. *Physical Review Letters* **108** (2012).
25. Zeng, H. L., Dai, J. F., Yao, W., Xiao, D. & Cui, X. D. Valley polarization in MoS_2 monolayers by optical pumping. *Nature Nanotechnology* **7**, 490–493 (2012).
26. Mak, K. F., He, K. L., Shan, J. & Heinz, T. F. Control of valley polarization in monolayer MoS_2 by optical helicity. *Nature Nanotechnology* **7**, 494–498 (2012).
27. Lebegue, S., Pillet, S. & Angyan, J. G. Modeling spin-crossover compounds by periodic DFT+U approach. *Phys. Rev. B* **78** (2008).
28. Ramasubramaniam, A. Large excitonic effects in monolayers of molybdenum and tungsten dichalcogenides. *Phys. Rev. B* **86** (2012).
29. Li, T. S. & Galli, G. L. Electronic properties of MoS_2 nanoparticles. *Journal of Physical Chemistry C* **111**, 16192–16196 (2007).
30. Kuc, A., Zibouche, N. & Heine, T. Influence of quantum confinement on the electronic structure of the transition metal sulfide TS_2. *Phys. Rev. B* **83** (2011).
31. Ramasubramaniam, A., Naveh, D. & Towe, E. Tunable band gaps in bilayer transition-metal dichalcogenides. *Phys. Rev. B* **84** (2011).
32. Ding, Y. et al. First principles study of structural, vibrational and electronic properties of graphene-like MX_2 (M = Mo, Nb, W, Ta; X = S, Se, Te) monolayers. *Physica B-Condensed Matter* **406**, 2254–2260 (2011).
33. Wildervanck, J. C. & Jellinek, F. Preparation and crystallinity of molybdenum and tungsten sulfides. *Zeitschrift Fur Anorganische Und Allgemeine Chemie* **328**, 309–318 (1964).
34. Khoo, K. H., Mazzoni, M. S. C. & Louie, S. G. Tuning the electronic properties of boron nitride nanotubes with transverse electric fields: A giant dc Stark effect. *Phys. Rev. B* **69** (2004).
35. Li, H. et al. From Bulk to Monolayer MoS2: Evolution of Raman Scattering. *Advanced Functional Materials* **22**, 1385–1390 (2012).
36. Mead, D. G. & Irwin, J. C. Long wavelength optic phonons in WSe_2. *Canadian Journal of Physics* **55**, 379–382 (1977).
37. Bonneau, P. R., Jarvis, R. F. & Kaner, R. B. Rapid solid-state synthesis of materials from molybdenum-disulfide to refractories. *Nature* **349**, 510–512 (1991).
38. James, P. B. & Lavik, M. T. Crystal structure of $MoSe_2$. *Acta Crystallographica* **16**, 1183–& (1963).
39. Clark, S. J. et al. First principles methods using CASTEP. *Zeitschrift Fur Kristallographie* **220**, 567–570 (2005).
40. Ceperley, D. M. & Alder, B. J. Ground-State of The Electron-Gas by a Stochastic Method. *Physical Review Letters* **45**, 566–569 (1980).
41. Perdew, J. P. & Zunger, A. Self-Interaction Correction to Density-Functional Approximations for Many-Electron Systems. *Phys. Rev. B* **23**, 5048–5079 (1981).
42. Ortmann, F., Bechstedt, F. & Schmidt, W. G. Semiempirical van der Waals correction to the density functional description of solids and molecular structures. *Phys. Rev. B* **73** (2006).
43. Perdew, J. P. et al. Atoms, Molecules, Solids, And Surfaces-Applications of the Generalized Gradient Approximation for the Exchange and Correlation. *Phys. Rev. B* **46**, 6671–6687 (1992).
44. Mahaha, S. K., Patel, K. D. & Menon, K. S. R. Electronic structure investigation of MoS2 and $MoSe_2$ using angle-resolved photoemission spectroscopy and ab initio band structure studies. *Journal of Physics-Condensed Matter* **24** (2012).
45. Refson, K., Tulip, P. R. & Clark, S. J. Variational density-functional perturbation theory for dielectrics and lattice dynamics. *Phys. Rev. B* **73** (2006).

Acknowledgements

Author contributions

H.T. proposed the idea, performed calculations and wrote the manuscript. F.L.U. performed calculations, discuss the results and revised the paper. M.T. discussed the results, contributed with ideas and wrote the manuscript.

Additional information